Empirical evidence reveals the phase diagram of vegetation patterns in Mediterranean drylands

Fernando Meloni[1,*], Gilberto M. Nakamura[1], Cristiano R. F. Granzotti[1], and Alexandre S. Martinez[1,2]

[1]Faculdade de Filosofia, Ciências e Letras de Ribeirão Preto, Universidade de São Paulo, Avenida dos Bandeirantes, 3900, 14040-901, Ribeirão Preto, SP, Brazil

[2]Instituto Nacional de Ciência e Tecnologia em Sistemas Complexos, Rio de Janeiro, RJ, Brazil

[*]Corresponding author: fernandomeloni@usp.br

ABSTRACT

Drylands are important ecosystems with limited water resources, often subject to desertification. Their ecological activities depend on spatial patterns formed by local vegetation, but the relation with vegetation growth remains unclear. Using satellite images of a typical semiarid shrubland in Southern Spain, we gather vegetation data and argue that vegetation cover can be interpreted by means of a percolation process. We use a static analysis that compares patch statistics in different spatial scales to study the various patch patterns that occurs in drylands. Our results indicate three distinct phases in the overall vegetation cover range. The spatial patterns of vegetation are separated by a first- and a second-order phase transition, in three different spatial scales. We measure the corresponding critical exponents and determine novel relations between scaling exponents. The results reconcile conflicting views about vegetation patterns in drylands and demonstrate that different phase transitions coexist in the phase diagram of dry shrublands in Southern Spain. In addition, our preliminary test with a distinct dryland supports the hypothesis of universality classes to sort different drylands.

Introduction

Drylands are arid and semiarid regions covering approximately 40% of the global landmass in which billions of people live. Vegetation in dryland ecosystems occurs in small clusters of plants intercalated by bare soil areas, respectively known as patches and inter-patches. The spatial arrangement of patches[1–3] is important to the ecosystem functionality as a whole, affecting soil stability, water runoff, and water absorption.[4,5] Small perturbations of the spatial structure of patches may lead to abrupt changes in the ecological structure. These changes are linked to the desertification process and may incur economic, environmental and social effects.[2,3,6–9] As a result, several studies have used empirical data and theoretical models to detect and forecast catastrophic shifts in vegetation patterns. Despite advances in this subject, there is a lack of consensus on the mechanism that causes the formation of the spatial patterns in drylands.[10,11] One approach employs statistical analysis of empirical data and shows that patch size distributions are well described by power laws or truncated power laws in several drylands.[12–18] Numerical simulations with *a priori* plant–plant interaction support these findings and reproduce typical patch patterns observed in drylands.[12,19,20] This approach highlights plant–plant interactions (facilitation and competition) and underestimates the influence of terrain features on vegetation patterns.[11] Other approaches state the importance of environmental conditions as the drivers of drylands vegetation and their spatial patterns. This view assumes that patch sizes exhibit a characteristic scale,[1,21,22] which questions the role of plant–plant interactions on pattern

formation. Empirical results mainly from Mediterranean drylands (MDL) support patch size distribution deviating from power laws, suggesting that terrain features are relevant.[11,23,24] As suggested in Meloni *et al.*,[24] plant–plant and plant–environment interactions seem to work together to produce vegetation patterns in drylands. In fact, theoretical models[2] and recent data[25] show that ecological conditions affect the spatial structure of vegetation, with consequences for the ecosystem functionality. However, the quantitative balance between such influences and the best manner in which to evaluate them remains poorly known for field conditions.

Central to this discussion is whether we can sort the various spatial patterns of vegetation into a reduced, more tractable, number of groups that share common properties. These groups are familiar in the physical sciences and denote thermodynamical phases or, simply, phases. In this context, a single phase labels numerous distinct spatial configurations of patches, similar to the ice phase that describes any crystalline configuration of water molecules. Thus, a proper description of drylands requires a phase diagram, which encompasses all phases available to the system and the transitions between each phase. For exploratory studies, phase transitions are crucial ingredients; they emerge whenever fundamental changes occur in the properties of the system, producing an effective way to outline the phase diagram. Two kinds of phase transitions, namely, first- and second-order phase transitions, concern us. In a first-order phase transition, the system undergoes a dramatic transformation between two distinct phases, which effectively changes the natural scale as the system transforms from one phase to another (for instance, the boiling of liquid water at 1 atm). Hence, first-order phase transitions are scale dependent and are always accompanied by discontinuities in the first derivative of the relevant statistics (order parameter).[26] In drylands, the abrupt desertification of vegetated regions with decreasing water availability suggests a first-order phase transition.[27] In second-order phase transitions, phases become indistinguishable from each other at the critical point,[26,28] where the transition takes place. In addition, the variance acquires an unusually large value. The theory of critical phenomena[26] states that fluctuations at all length scales produce these abnormal values, rather than only those at a single scale. As a consequence, the relevant properties near criticality are scale invariant, *i.e.*, they are well described by power laws and their critical exponents. For drylands, this outcome is in agreement with previous studies concerning vegetation patterns in MDL.[12–18]

Here, we avoid the statistical distribution debate and adopt an alternative approach to address the MDL phase diagram and the role of plant–plant and plant–environment interactions in the formation of patch patterns. Vegetation patterns are explained as the result of a percolation process at three different spatial scales, in which the terrain plays a crucial role. This approach allows us to link the connectedness of patches with the terrain features and to classify the phase transitions in the overall vegetation cover range. Critical exponents of the second-order phase transition are estimated, and new relations between the scaling exponents are determined analytically and validated by empirical data. We offer evidence about terrain effects on patch continuity, and we discuss the ecological framework linking the phase diagram, the coalescence process and ecohydrological aspects. We argue that this approach offers new insights into the management of dryland ecosystems.

To contextualize this work, we note here that this study regards the vegetation patterns of drylands located in Southern Spain, within the Murcia municipality (see Methods), which we refer to here simply as MDL (Mediterranean drylands). Vegetation data were collected from Google Earth images with a resolution of < 40 cm (see Figs. 1 and 2) and are grouped into three sets of images. Each set contains non-overlapping and independent images of square regions, the plots, with sides of length $L_1 = 5$ m (29 images), $L_2 = 10$ m (42 images) and $L_3 = 30$ m (40 images), with corresponding areas $A_i = L_i \times L_i$ m^2. Each plot is uniquely identified by its image label and area. The plot images have the pixel as the basic unit of measure. Each pixel represents the same length (in meters) for plots of different scales, so that images in different scales only differ in the total number of pixels. The plot images are manually processed by color filtering using the ImageJ software[29] as described in Ref.[24] (see Methods).

Afterwards, the filtered images are transformed to binary images, where each pixel can either take the value 1 (filled by vegetation) or 0 (empty). For binary images, a single patch is a cluster of filled pixels surrounded by empty pixels. With ImageJ analytical tools, it was possible to identify, count and measure each patch present in each plot. To avoid any inferences from the vegetation growth, we restricted our analysis only to static properties measured for each plot. The control parameter is the vegetation cover $0 \leq V \leq 1$, *i.e.*, the relative amount of vegetation covering one plot, and the following quantities are extracted directly from the binary images of each plot:

- $N(V)$ is the number of patches, and $D(V) = N(V)/A$ is the patch density;
- $\hat{\mu}(V)$ is the average size of the patches, and $\hat{\sigma}^2(V)$ is the corresponding variance;
- P_{max} is the largest vegetation patch;
- $P(V)$ is the probability that a random filled pixel belongs to P_{max}, and
- $J(V) = P_{max}/A$ is the probability that a random pixel belongs to P_{max}.

From the patch statistics, additional variables are estimated:

- V_m and V_c are the V values at which the first- and second-order phase transitions take place;
- α and β are critical exponents;
- δ, γ and ρ are scaling exponents;
- z is the coordination number of a Bethe lattice,[30] related to the patch connectivity.

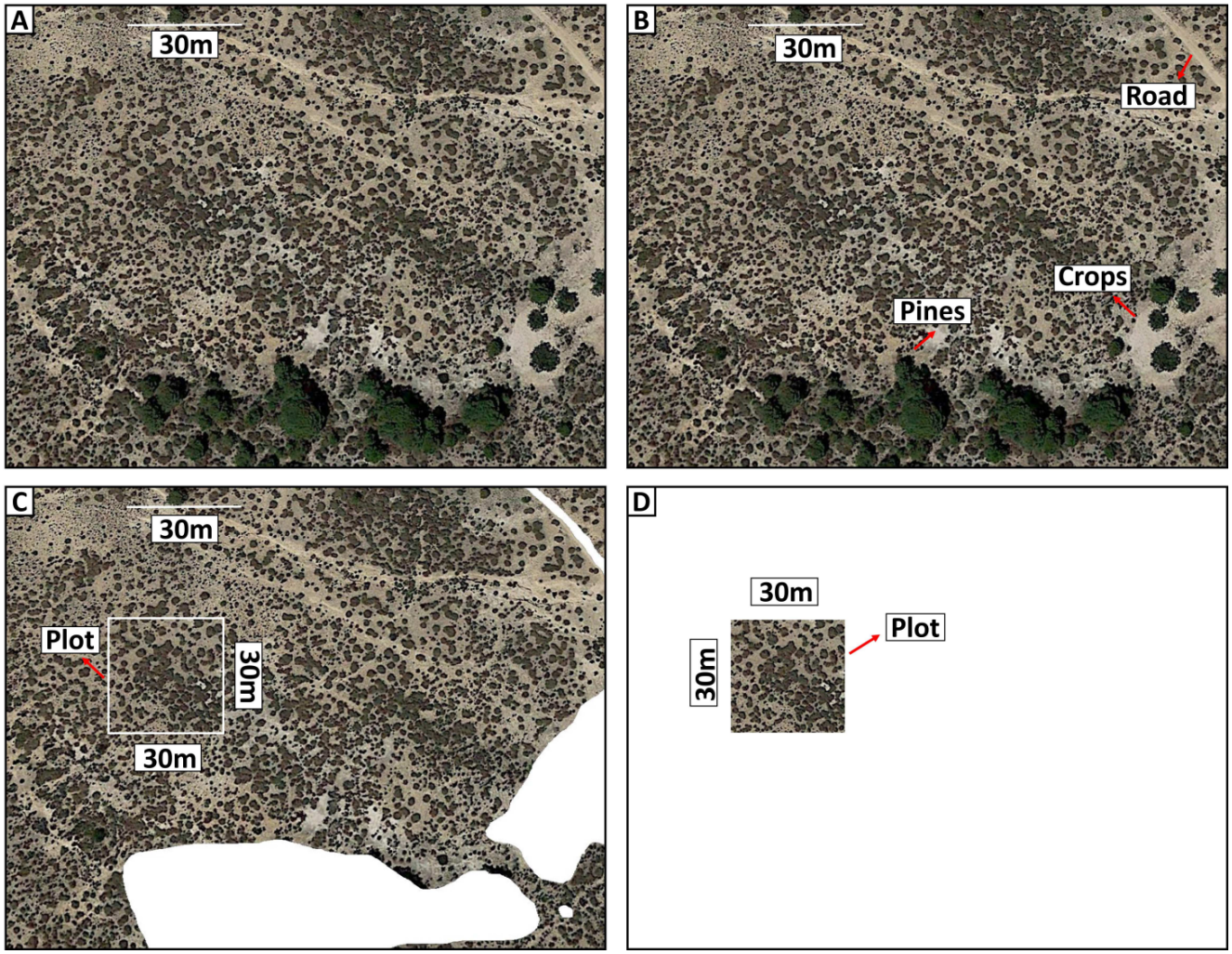

Figure 1. Steps to obtain a plot from Google Earth. The plot is an image sample obtained from Google Earth, which represents the typical vegetation, the "Espartales", found in the region. To find plots, a random search was done through the landscape (view altitude ≈ 200 m), seeking to detect a region containing (almost exclusively) the target vegetation. (**A**) An adequate region is detected and a raw image is acquired. (**B**) Each element in the landscape is identified. (**C**) All undesired elements (such as crops, roads, buildings, etc) are avoided before defining the plot. (**D**) A sample image of "Espartales", namely, the plot, is obtained. Each plot is acquired independently from the others, and they are only identified by their respective labels and areas (m^2).

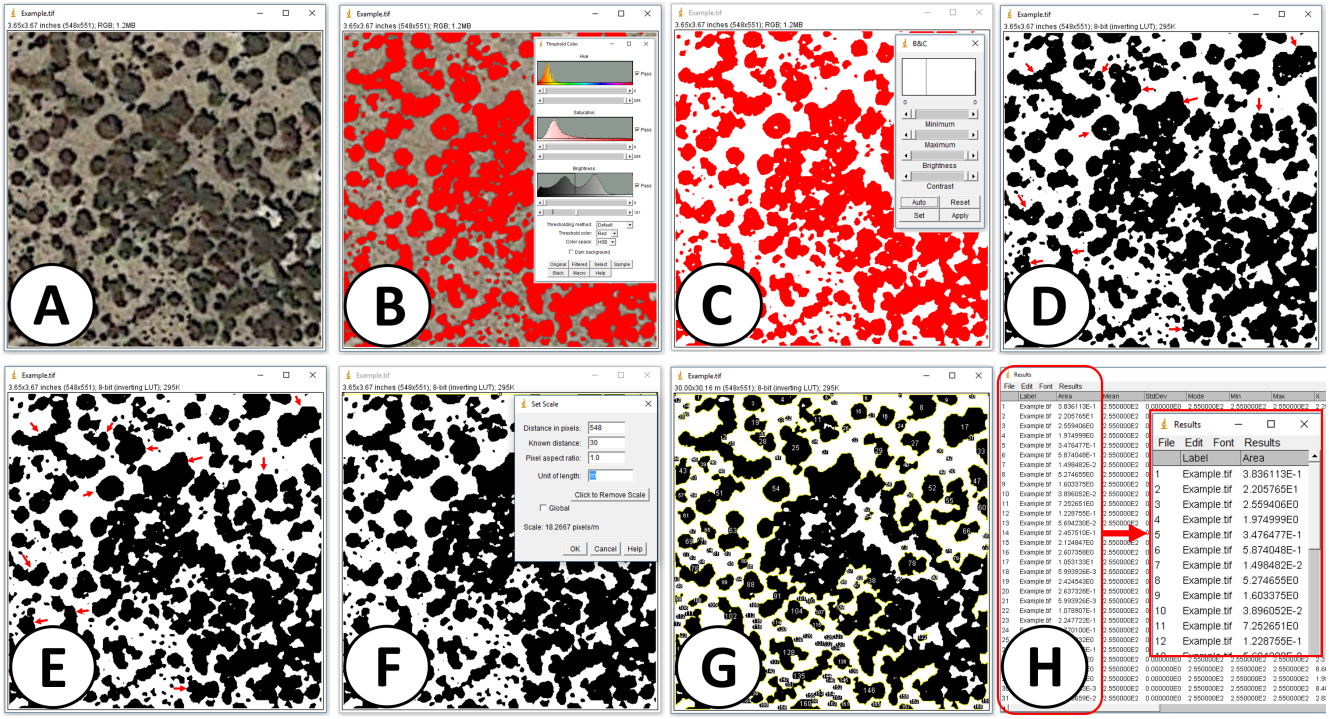

Figure 2. Steps to process the plot images and the statistics obtained from each plot. All image processing is performed with ImageJ tools,[29] under human supervision. Images A–H depict the windows shown by ImageJ during the process. A: The plot is defined as a small image obtained from Google Earth and represents exclusively the "Espartales", a typical vegetation physiognomy found in the region. Each plot is spatially independent from the others and is identified only by a label and its respective area scale. In this figure, the plot is labeled "Example", and it measures $30 \times 30m^2$. B: Color filtering is used to separate vegetation from bare soil. C: Brightness filtering is applied, separating the background (bare soil) from red regions (vegetation). D and E: The colored images (filtered) are transformed into binary images, where vegetation and bare soil are represented by black and white pixels, respectively. Depending on the image, large patches may exhibit high brightness, low contrast, or excessive shades, or the terrain may show some particular feature, which can reduce the quality and exactness of the binary image compared to the plot image. Such imperfections are hand-corrected using the editing tool after examining both images (see red arrows). F: The pixel density is determined after setting the scale (L_1, L_2 and L_3). G: ImageJ analytical tools are applied to find patches (clusters of black pixels completely surrounded by white pixels) and measure them. H: Several raw measures of patches are obtained and exported as an *.xls* file, allowing the determination of several statistics. In this example, $V \approx 0.52$, $\hat{\mu}(V) \approx 2.75m^2$, $\hat{\sigma}^2(V) \approx 297.7$, $N(V) = 160$, $D(V) \approx 0.19$, $P(V) \approx 0.48$, and $J(V) \approx 0.25$.

Results

Fig. 3(A) depicts $\ln N(V)$ for the three plot sizes (L_1, L_2 and L_3). These curves are rescaled by using a single variable, $\ln D(V)$, shown in Fig. 3(B). Both cases clearly demonstrate the existence of two different phases, separated by the transition point $V = V_m \approx 0.4$ obtained at the largest scale (L_3). For low vegetation cover, $V < V_m$ (Phase A), the patches are small and randomly scattered on the plot (patch coalescence is rare). At $V = V_m$, patch coalescence emerges as the dominant process, leading to a fast reduction in patch numbers for $V > V_m$ (Phase B). Fig. 3(B) also depicts all curves collapsing for $V \leq V_m$, but not for for $V > V_m$, confirming the scale dependence. The scale dependence excludes any possibility of a second-order phase transition. Instead, it is typical signal of first-order phase transitions. Furthermore, the abrupt decrease in $\ln D(V)$ is another classic signature, providing conclusive evidence.[26] Concerning the percolation analysis, Fig. 3(C) shows that $J(V)$ also experiences a sudden change at $V_m \approx 0.4$, in accordance with the first-order phase transition evidenced by $D(V)$. As expected, the scale L_1 always presents larger deviations, although the rescaled curves suggest great coherence among the curves obtained from different plot sizes.

The normalized $\hat{\sigma}^2(V)$ is depicted in Fig. 4 to show that a second-order phase transition could be present in the phase diagram. Since $\hat{\sigma}^2(V)$ vanishes for $V = 0$ and $V = 1$, one would expect at least one peak or divergence in the interval $V \in (0,1)$. According to the data, the collapsed curves $\hat{\sigma}^2(V)$ vanish for $V \leq V_m$, rapidly increase for $V > V_m$, reach unity for $V = V_c \approx 0.8$, and vanish for $V > V_c$. Indeed, at $V = V_c$, the probability $P(V)$ reaches a stable value, meaning that P_{max} reaches the size of the system. Consequently, most of the filled pixels belong to the largest patch in the plot when $V = V_c$, which depicts the transition separating Phase B from Phase C. The phase transition captured by $\hat{\sigma}^2(V)$ is indicated by a prominent peak (divergence), where the maximum values are achieved at V_c and vanish for $V > V_c$. This "divergence" is indicative of a second-order phase transition taking place at $V = V_c$. To ensure that the transition is second order, the divergence of $\hat{\sigma}^2(V)$ at V_c (critical point) must be found in all plot scales (scale invariance). This requirement justifies our choice to employ three plot sizes. As depicted in Fig. 4, the curves of the three considered scales collapse, with their respective $\hat{\sigma}^2(V)$ values diverging around $V = V_c$, providing the final evidence. The transition is attributed to the crescent coalescence at $V_m < V < V_c$, indicating that patch continuity reaches its maximum at $V \geq V_c$. For V near V_c, biological effects on spatial patterns and ecological dynamics, such as plant–plant interactions, cannot be neglected (see Discussion).

With this confirmation of a second-order phase transition, several inferences can be taken from critical phenomena theory[26,31] (see Discussion). In the scaling region (vicinity of the critical point), $\hat{\sigma}^2(V)$ is scale free and is then well described by a power law, whose exponents are known as the critical exponents. Hence, we mapped the pertinent quantities from MDL to their corresponding thermodynamical quantities around the critical transition. In this context, $\hat{\mu}(V)$ plays the role of the order parameter, while $\hat{\sigma}^2(V)$ measures the corresponding fluctuation. In the immediate vicinity of V_c, both observables scale as

$$\hat{\mu}(V) \sim |V - V_c|^{-\alpha} \text{ and} \tag{1}$$

$$\hat{\sigma}^2(V) \sim |V - V_c|^{-\beta} . \tag{2}$$

In Figs. 5(A) and (B), we depict collapsed data from the 3 different plot sizes, and the critical exponents are estimated using linear fits in the log-log scale:

$$\alpha = 0.4 \pm 0.2 \text{ and} \tag{3}$$

$$\beta = 0.5 \pm 0.5 . \tag{4}$$

Eqs. 1 and 2 are subject to systematic errors due to improper identification of the scaling region.[32] These systematic errors become progressively significant with data reduction or insufficient vegetation coverage. As a consequence,

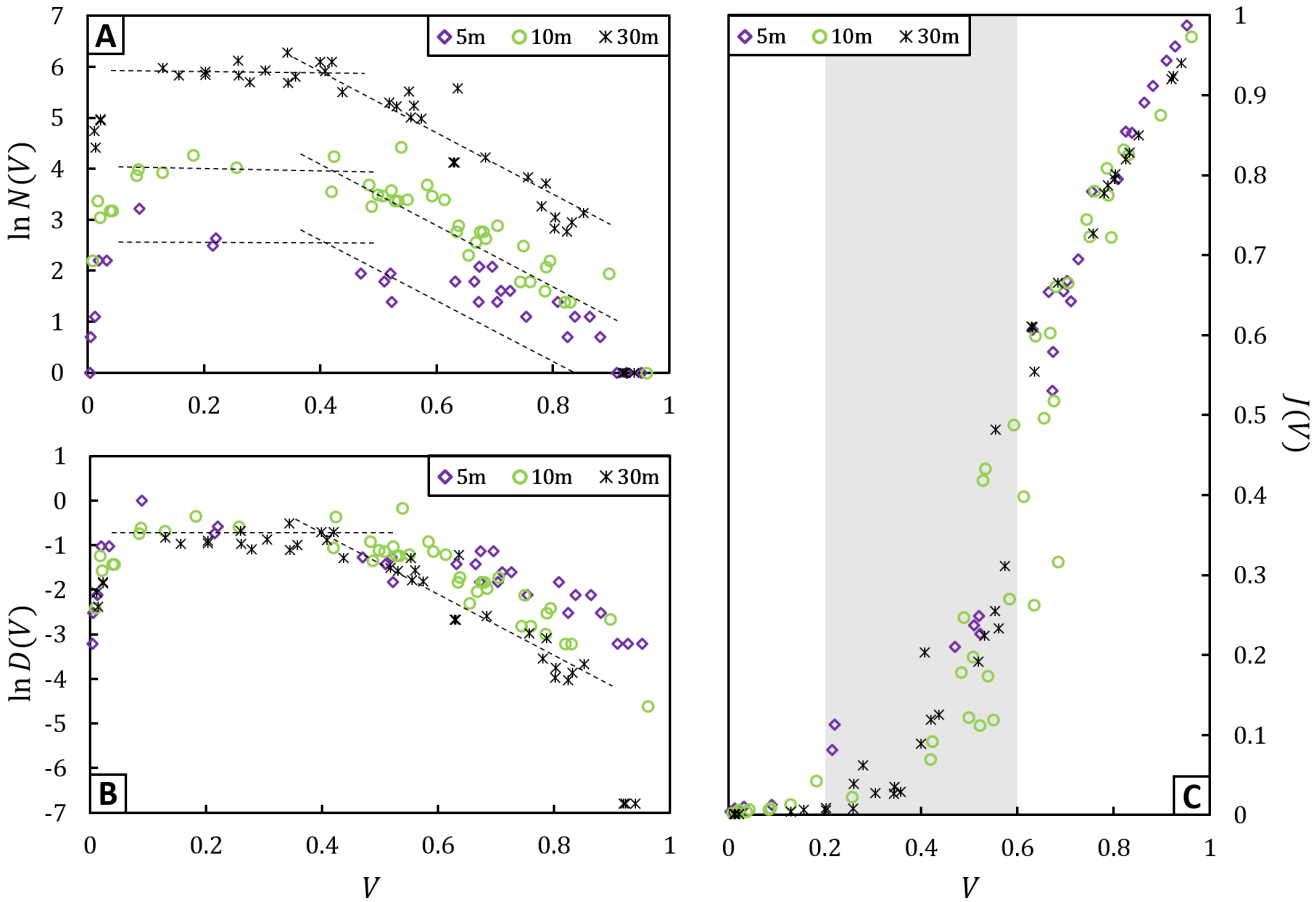

Figure 3. Patch statistics describing the geometrical properties of patch patterns in MDL. Dashed lines are visual guide lines; V: vegetation cover; $N(V)$: number of patches; $D(V)$: patch density; $J(V)$: the probability that a random pixel belongs to the largest patch. **(A)** Curves of $\ln N(V)$, at three different spatial scales: $L_1 = 5$ m, $L_2 = 10$ m and $L_3 = 30$ m. The behavior of each curve suddenly changes around $V_m \approx 0.4$ due to the rapid decrease in $N(V)$ in a plot. **(B)** $\ln D(V)$ of distinct plot sizes show moderate coherence with a single curve for $V \leq V_m$, but they clearly show discrepant tendencies for $V > V_m$, indicating scale dependence; **(C)** $J(V)$ collapsed data demonstrating the existence of a transition centered at $V_m \approx 0.4$ (shaded region). Such behavior of $\ln D(V)$ and $J(V)$ excludes the second-order phase-transition hypothesis and reinforces the plausibility of a first-order phase transition at the vicinity of $V_m \approx 0.4$. Despite the good collapse of $\ln D(V)$ and $J(V)$, the data for scales L_1 and L_2 exhibit large fluctuations compared to L_3.

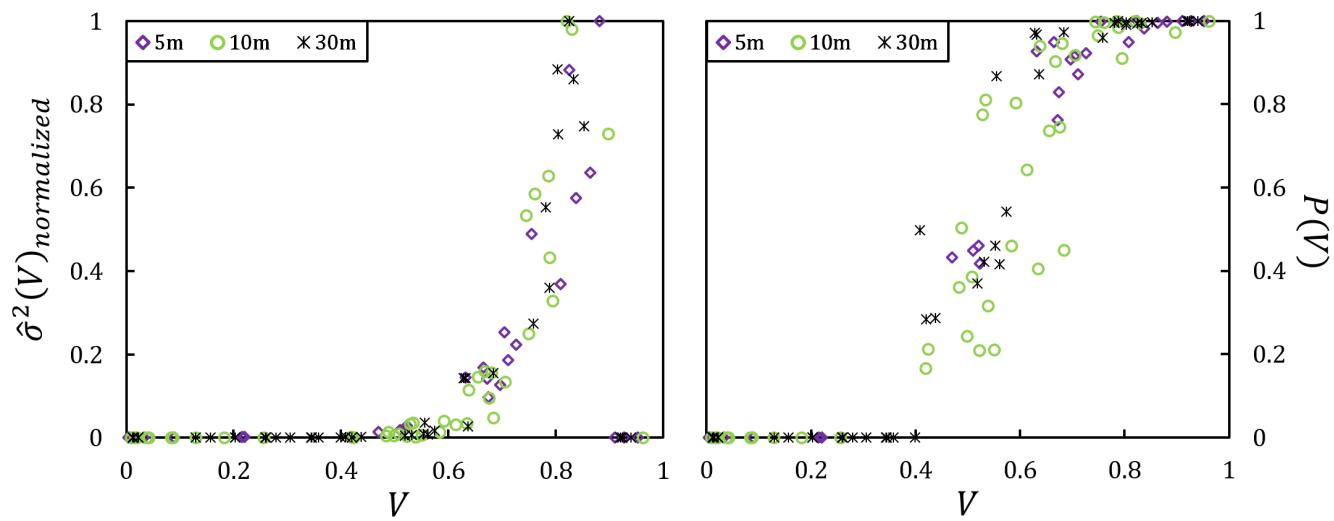

Figure 4. Patch-size normalized variance $\hat{\sigma}^2(V)$ of plots taken at three distinct scales, $L_1 = 5$ m , $L_2 = 10$ m and $L_3 = 30$ m (left). The $\hat{\sigma}^2(V)$ divergence at a vegetation cover $V = V_c \approx 0.8$ indicates a second-order phase transition. The probability of a random vegetated pixel belonging to the largest patch $P(V)$ (right). For $V > V_c$, all patches belong to the largest patch (giant component) with $P(V) = 1$, while $\hat{\sigma}^2(V) = 0$. In both cases, the curves practically vanish for $V < V_m$ but increase rapidly in the range $V_m \leq V \leq V_c$, indicating the emergence of patch coalescence at $V \approx V_m$.

we observe large deviations in the estimates of critical exponents and small fit confidence. We mitigate this issue by considering more reliable scaling laws among the variables

$$\hat{\mu}(V) \sim [D(V)]^{-\Delta}\,, \tag{5}$$

$$\hat{\sigma}^2(V) \sim [D(V)]^{-\gamma} \text{ and} \tag{6}$$

$$\hat{\sigma}^2(V) \sim [\hat{\mu}(V)]^{\rho}\,, \tag{7}$$

where the scaling exponents Δ, γ and ρ are again estimated using linear fits in log-log scales. Since Eqs. 5, 6 and 7 are valid only in the scaling region, one can continuously decrease V starting from $V = V_c$ for each plot scale L, as long as these equations hold. This procedure allows for a more accurate estimation of the scaling region (higher R^2) than using Eqs. 1 and 2. In Fig. 5(C), (D) and (E), the scaling exponents are

$$\Delta = 1.1 \pm 0.1\,, \tag{8}$$

$$\gamma = 1.3 \pm 0.3 \text{ and} \tag{9}$$

$$\rho = 1.2 \pm 0.2\,. \tag{10}$$

First, the scaling relations in Eqs. 5, 6 and 7 are consistent if $\rho = \gamma/\Delta$. Next, substituting Eqs. 1 and 2 in Eq. 7 produces $\hat{\sigma}^2 \sim |V - V_c|^{-\beta} \sim |V - V_c|^{-\rho\alpha}$, and hence, $\beta = \rho\alpha$. These predictions for β and ρ are then compared to the corresponding values obtained directly from empirical data. Here, we test the scaling relation $\rho = \gamma/\Delta = 1.2 \pm 0.2$, which is compatible with the value obtained from the empirical data. Furthermore, the alternative estimation $\beta = \alpha\rho = 0.52 \pm 0.50$ is in accordance with the values obtained by the direct fit.

Finally, the assessment of vegetation connectedness requires percolation analysis, including the substrate where the percolation takes place. For that purpose, we employ a simplified representation for the terrain structure as a Bethe lattice, which is a tree-like recursive structure without loops and coordinate number z. The procedure allows

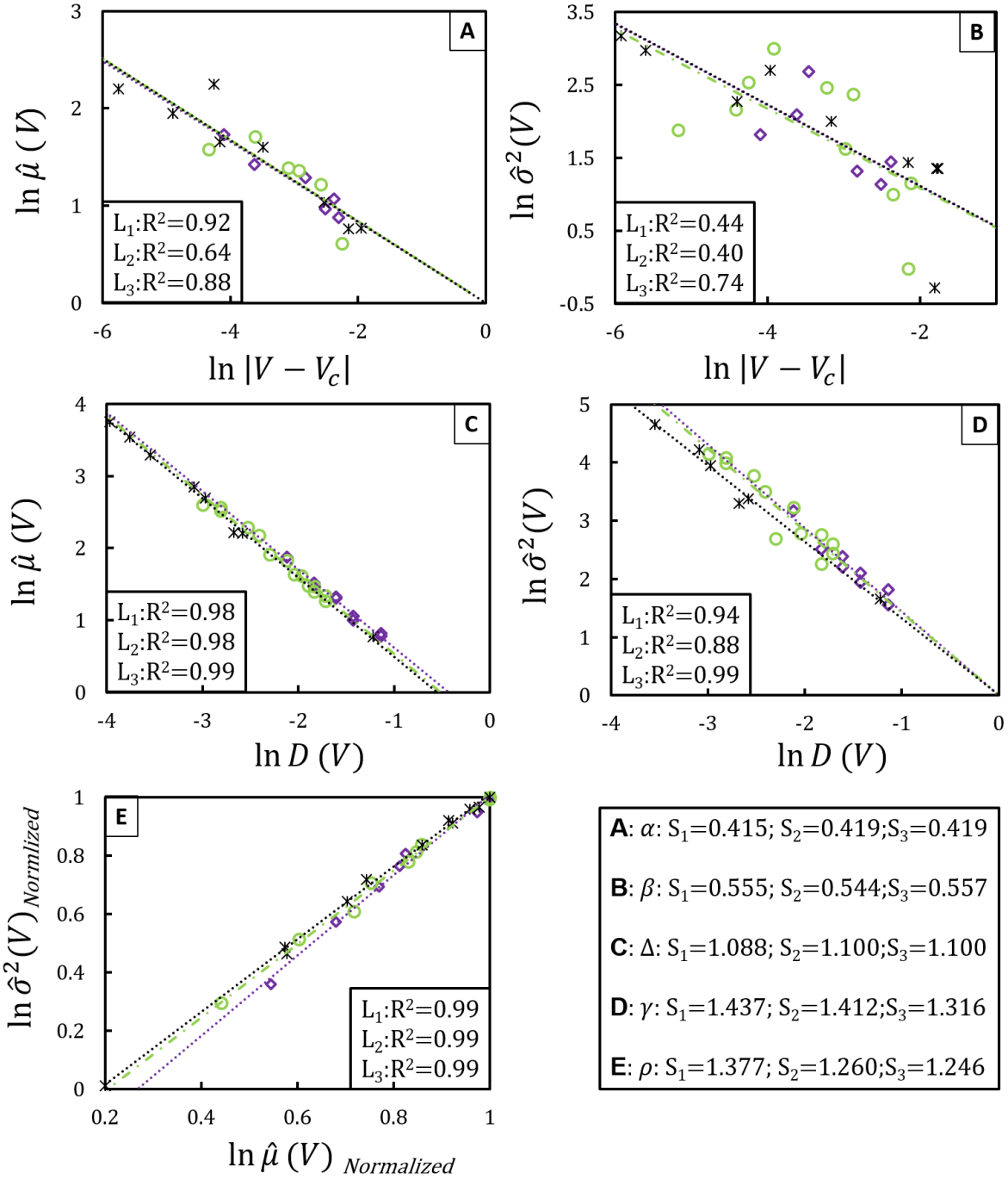

Figure 5. Relationship between scaling and critical exponents observed in dry shrublands of south Spain at three distinct scales: $L_1 = 5$ m, $L_2 = 10$ m and $L_3 = 30$ m. The analysis only uses data from plots with V values in the vicinity of the critical transition ($V = V_c \approx 0.8$) to estimate the exponents of Eqs.3, 4 and Eqs.5–7 using a linear fit at a log-log scale. **(A)** Critical exponent $\alpha = 0.4 \pm 0.2$ of the patch size average, Eq.3; **(B)** Critical exponent $\beta = 0.5 \pm 0.5$ of the patch size variance, Eq.4; **(C)** Scaling exponent $\Delta = 1.1 \pm 0.1$ of the patch size average; **(D)** Scaling exponent $\gamma = 1.3 \pm 0.3$ and **(E)** Scaling exponent $\rho = 1.2 \pm 0.2$ of the patch size variance, Eqs.6 and 10.

us to obtain a coarse-grain estimation of the terrain connectivity and vegetation connectedness. The minimum connectivity necessary for percolation is $z = 3$, for which the transition takes place at $V \to 1$. For $z > 3$, the percolation takes place at smaller V values.[30,31] This assumption allows for the calculation of relevant quantities and statistics based on geometrical properties of the system. For instance, z is evaluated from[30]

$$V_m(z-1) = 1, \tag{11}$$

which results in $z = 3.5$ for our data. With z in hand, one calculates $1 - J$[30]

$$1 - J(V) = (1 - V) + [1 - J(V)]^{z-1}. \tag{12}$$

Alternatively, the probability $1 - J$ may also be estimated from raw data and compared against the value from Eq. 12, as depicted in Fig. 6. The comparison produces excellent agreement throughout the entire V range and for all plot sizes. Therefore, despite possible inaccuracy in modeling the patch structure as a Bethe lattice, the inferences about connectivity are supported by the data available. These results indicate that patches are poorly connected for the entire V range and that conditions for vegetation growth are always heterogeneous in MDL. A homogeneous terrain would be implied by $z = 4$, with each filled pixel connecting to four other filled pixels, meaning that all regions in the plot are permissive to patch growth. Consequently, the calculated connectivity, $z = 3.5$, is smaller in MDL than in a homogeneous terrain. In turn, some regions of bare soil are very resilient and persist even for large V values. Therefore, our results provide strong evidence supporting the importance of terrain constraints for vegetation growth and, consequently, for the formation of the patch structure.

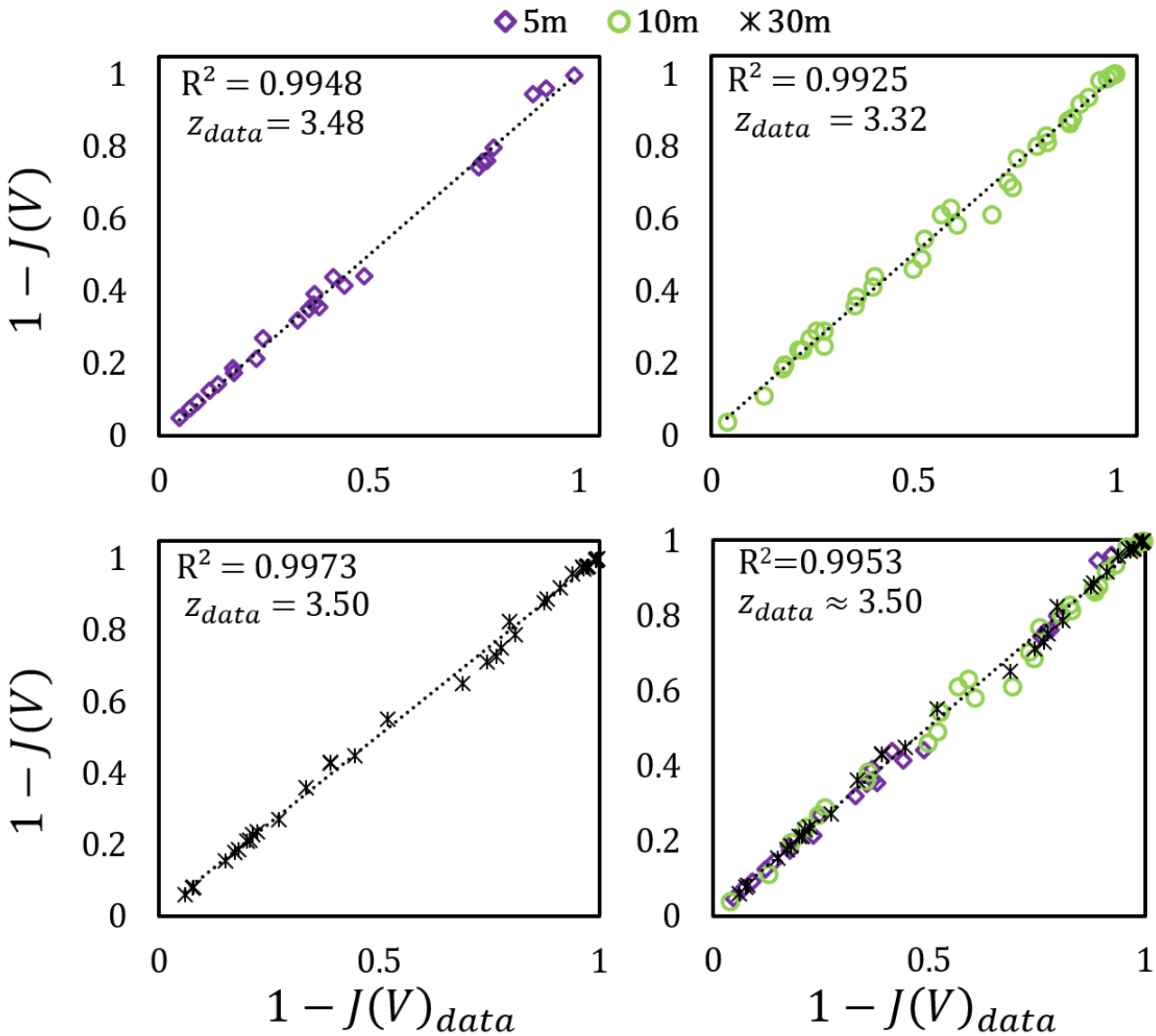

Figure 6. Vegetation of dry shrublands in south Spain as a percolation process in a Bethe lattice. $1-J(V)_{data}$ is the probability that a random site does not belong to the largest patch obtained from empirical data. The prediction $1-J(V)$ is found with Eq.12 where the coordination number z may be estimated by both Eq.11 and the probability $1-J(V)_{data}$. z refers to the patch connectivity and terrain features; the low connectivity ($z \approx 3.5$) implies spatial constraints for patch growth. The values of z and $1-J(V)$ calculated by the different methods are compatible in the three scales, supporting the inferences about terrain connectivity obtained from the model.

Discussion

Our findings show that the investigated MDL supports three distinct vegetation patterns, namely, phases A, B and C, according to the control parameter V. They are separated by a first-order ($V_m \approx 0.4$) and a second-order ($V_c \approx 0.8$) phase transition as V increases from zero to unity (see Fig. 7).

This scenario contrasts with those furnished by traditional models for drylands; some models predict only a first-order phase transition, separating a desertified phase from a completely vegetated phase, while others consider only the second-order phase transition to be viable.[2,12,17,27,33–35] Moreover, theoretical models concerning self-organization and terrain effects can qualitatively indicate more transitions.[36,37] However, none of the aforementioned models reproduce the results we presented here. Therefore, by showing that a first- and second-order phase transition coexist in the phase diagram depending on V, our findings offer strong evidence capable of unifying apparently conflicting research lines and reconciling disparate views about the vegetation patterns in drylands.

Phase transitions

Scarce and small patches compose Phase A ($V < V_m$), which hinders water infiltration and favors runoff effects.[4,5,38] Due to their smallness, the patches are randomly scattered across the landscape, producing short range-correlations (characteristic scale). This observation is supported by previous studies in the same region using patch size distributions.[23,24] Therefore, facilitation effects are less important in phase A, and terrain influences dominate the vegetation growth (new colonizations and peripheral increment around already established patches). In fact, the most abundant plant species in the region, the alpha grass *Stipa tenacissima* L., grows as mentioned above. As V increases towards V_m, one also expects the number of patches and their corresponding average size to increase. However, with increasing sizes, nearby patches are more likely to coalesce, reducing the total number of patches. Of note, first-order phase transitions are mainly governed by terrain and climate conditions, which affects the V_m threshold.

Phase B occurs within the range $V \in [V_m, V_c]$. Unlike in the other two phases, the spatial arrangement of patches lacks a simple characterization in phase B. The issue with the characterization of Phase B is reported by Aguiar and Salas.[39] The authors recognize two phases, low and high cover, for several worldwide drylands with evident differences in spatial patterns and ecological interactions. They describe the low-cover phase in a manner that fits Phase A, but they are unable to perform a simple description of the high-cover phase. In Phase B, the total number of patches decreases, and patches becomes larger in size. This is a consequence of coalescence, which also increases the variability of geometrical forms and shapes found in distinct plots. This constant competition for space during vegetation growth effectively produces a net increase in the variance of patches. In particular, the variance associated with Phase B develops a characteristic length scale that differs from the one from phase A. The changes in scale in drylands have been previously announced by von Hardenberg *et al.*[2] Among their results, they numerically verified that patch size distribution also develops distinct characteristic scales as the vegetation cover increases. The change in characteristic scale at V_m is in agreement with a first-order phase transition. Our evidence suggests that plant–plant interactions are not driving the vegetation growth during $V \sim V_m$ but that they gain importance as $V \to V_c$, an implication of coalescence. This means that changes in the spatial structure of vegetation during Phase B can be explained by neither terrain features nor plant–plant interactions alone.

In phase C, $V > V_c$, the vegetation reaches a continuous configuration (Fig. 7), prone to water infiltration and minimally affected by runoff. In general, this combination mitigates desertification threats. Moreover, the large levels of vegetation cover also lessen the influence of terrain compared to that of plant–plant interactions as the main regulator of vegetation patterns. Hence, the properties and characteristics of phase C contrast greatly with those of phase A. This contrast is also observed in the transition from phase B to C: the former is first order whereas

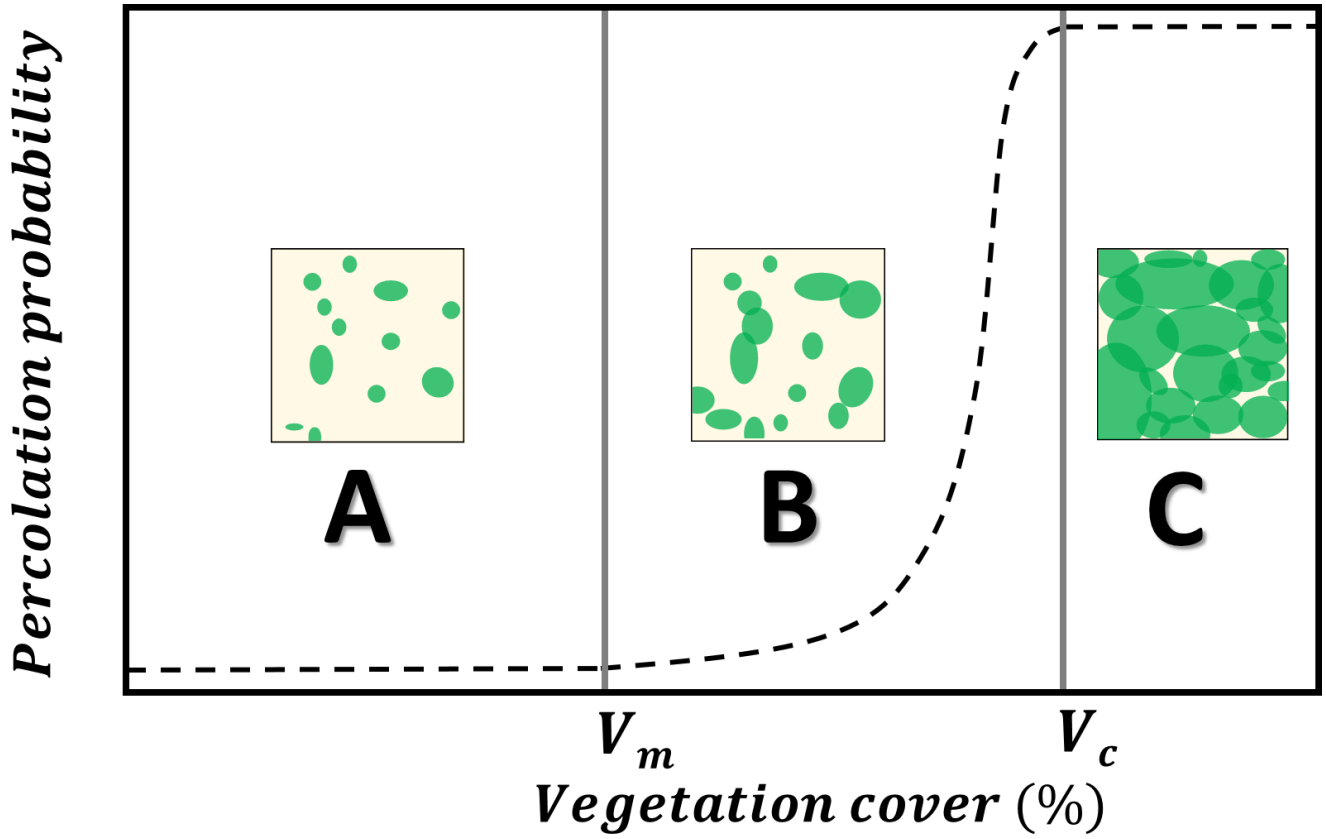

Figure 7. Phase diagram of dry shrublands in south Spain. The figure highlights the distinct spatial arrangement of patches at distinct ranges of vegetation cover V according to phases A, B and C. In regime **A**, the geometrical properties of patches show random patterns, with maximum effects of hydric runoff and minimum water infiltration in the soil. A first-order phase transition occurs at $V_m \approx 0.4$. In regime **B**, coalescence drives the growth of patches, affecting patch sizes and density in a non-trivial manner. The changes in the spatial arrangement result in a drastic increase in patch connectivity, with consequences for runoff and water infiltration. The coalescence process saturates at the emergence of a percolating vegetation patch, at $V_c \approx 0.8$, where a second-order phase transition drives the system from regime **B** to regime **C**. Such a transition is the remarkable consequence of long-range correlations, revealing the crescent-shaped relevance of biological interactions for the vegetation dynamics during regime **B**. In regime **C**, the fully connected vegetation patch mitigates the effects of runoff and improves water absorption, and terrain features show little relevance, while biological aspects dominate the effects on vegetation patterns.

the latter is second order. We stress that the nature of the B-C transition was determined from the divergent behavior of $\hat{\sigma}^2$ around the critical point V_c. Indeed, the theory of critical phenomena explains that the large value of $\hat{\sigma}^2$ is due to scale invariance, whose hallmark is the presence of long-range spatial correlations.[26,28,30,40,41] Our results for $\hat{\sigma}^2$ are in accordance with previous dryland studies.[12,13,17,19,42] For instance, Xu *et al.*[18] considered several drylands and observed an increase in the skewness of patch size distributions up to $V \approx 0.7$ in the empirical data. However, the authors were unable to assess large values of V, *i.e.*, they could not detect the critical phase transition. Here, we consider smaller plots because the vegetation coverage in drylands rarely exceeds 60% for large areas. This allows for a better assessment of the entire V range.

Bearing in mind the critical phase transition, we highlight the discovery of the scaling relations among $D(V)$, $\hat{\mu}(V)$ and $\hat{\sigma}^2(V)$. The equalities $\rho = \gamma/\Delta$ and $\beta = \rho\alpha$ relate the scaling exponents ρ, Δ and γ to the critical exponents α and β. This is the expected outcome in the classical theory of critical phenomena, and, as such, grants us confidence in the validity of the critical hypothesis. The experimental observation of a second-order phase transition is no minor feat. The reason behind this claim lies in another crucial concept of critical phenomena: universality classes.[40,41] This concept asserts the following. Distinct systems are grouped together and exhibit the same universal features provided they share the same critical exponents and symmetries. In the physical sciences, the broad term "distinct systems" refers to systems that may range from gases to magnets. In the ecological context, however, we are concerned only with different drylands subject to similar environmental filters. Thus, universality classes provide an ideal framework to investigate the underlying biological interactions in drylands.

For drylands with similar conditions and plant–plant interactions, one expects similar critical exponents, *i.e.*, that the various worldwide drylands would be grouped into a reduced number of universality classes. Recently, Berdugo *et al.*[25] provided empirical evidence that supports our hypothesis of dryland universality. The authors evaluated 115 dryland plots worldwide, searching for relations between aridity and system functionality. With these parameters, the authors sorted the dryland samples into two groups: a high aridity/low functionality data set, associated with a lognormal distribution for patch sizes, and a high functionality/low aridity data set, associated with power-law distributions. Our approach offers a simple interpretation of their previous findings. For instance, the link among functionality, aridity and patch size distribution[25,43] might be explained by the main aspects of the phase diagram reported here (scale-dependent phases and one scale-free phase transition). This inspired us to perform a preliminary test, employing the same methods used in MDL for drylands located in Utah, US (36 plots). In Utah, patches are constituted by trees associated with shrubs, a notable difference in comparison to the Spanish case. Nevertheless, Fig.8 depicts that normalized variances from MDL (30 m) and the US (50 m) collapse in a single curve, indicating the same behavior at a critical phase transition. Unexpectedly, the critical points in both drylands occurr at the same value, even though this is not a universal feature. Furthermore, the exponents found for US drylands are $\alpha_{\mathrm{US}} \approx 0.42$ and $\beta_{\mathrm{US}} \approx 0.46$, which fall under the expected errors of critical exponents from MDL (Supplementary Information). Therefore, this preliminary test supports our hypothesis of universality classes as a way to sort the various worldwide drylands.

MDL Management

The interpretation of the phase diagram found in our study (Fig. 7) may be also used to propose guidelines for the management of the assessed MDL regions. For this, it is necessary to consider the role of patch continuity in water infiltration and runoff effects[4,5,38,44,45] and interpret the correlation between patch patterns and ecosystem functionality. For instance, changes in vegetation cover result in small effects on ecosystem functionality in phases A and C because the amount of vegetation weakly affects the geometrical properties of the patches. However, the ecosystem functionality in Phase B depends on vegetation cover because the ecohydrological condition is directly

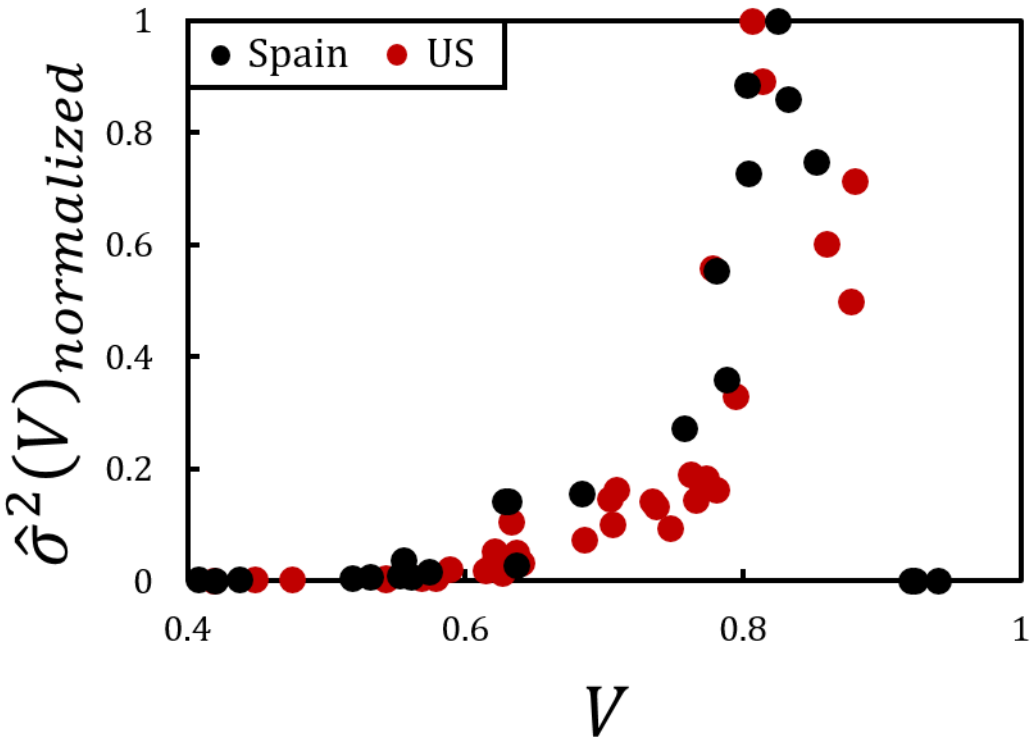

Figure 8. Preliminary test depicting the normalized patch-size variances $[\hat{\sigma}^2(V)]$ observed in two distinct drylands. Plots from Spain (black) show $L = 30$ m, while plots from US (dark red) show $L = 50$ m. In Spain the vegetation is mainly formed by shrubs, while in US the occurrence of shrubs is associate with trees. Despite the inherent ecological differences between both vegetations, their respective variances collapse into a single curve. A second-order phase transition is observed in the two drylands at $V = V_c \approx 0.8$. The values of critical exponents calculated for plots from US ($\alpha_{\mathrm{US}} = 0.42$; $\beta_{\mathrm{US}} = 0.46$) are compatible with values calculated for plots from Spain. This evidence reinforces the hypothesis that drylands might be classified in universality classes.

affected by vegetation continuity.

Thus, in Phase A, plots show small patches, water infiltration is low, and runoff is high, meaning that the ecosystem is more susceptible to environmental factors. Consequently, the desertification threat is high in Phase A. In phase C, the vegetation forms a continuum, which maximizes the water infiltration and minimizes the runoff effects. Therefore, Phase C shows the smallest influence from environmental factors, and the risk of desertification can be considered smaller than in the other configurations. The intermediate stage, Phase B, shows the most sensitive state, where the spatial configuration is determinant for the ecosystem stability. Our findings show that the chances of the system to become continuous in Phase B unevenly increase as V (exponentially) increases. Thus, plots with $V > V_m$ have a much higher chance to be recovered than plots with $V < V_m$, and also, small restoration efforts would lead to great increments in ecosystem functionality. In Ref.,[25] a bimodal relationship between vegetation cover and ecosystem functionality is found for drylands worldwide, meaning that the patterns reported here may be also present in other drylands.

These are early signals of catastrophic shifts in drylands. Although our study concerns data from a restricted region with its own constraints, we highlight that the approach we propose here can be applied to other dryland regions and that the transition values V_m and V_c can be altered, but not the critical exponents α and β or their relation with scaling exponents Δ, γ and ρ. Hence, we call attention to the necessity of mapping such thresholds for different dryland regions.

Conclusions

We report three vegetation regimes (Phases A, B and C) for Mediterranean drylands via the analysis of $D(V)$ and $\hat{\sigma}^2(V)$, using the vegetation cover V as control parameter. Phases A and B are separated by a first-order phase transition that takes place at $V = V_m \approx 0.4$. The transition between Phases B and C is second order and occurs at $V = V_c \approx 0.8$. The critical ($\alpha = 0.4 \pm 0.2$, $\beta = 0.5 \pm 0.5$) and scaling ($\Delta = 1.1 \pm .1$, $\gamma = 1.3 \pm 0.3$ and $\rho = 1.2 \pm 0.2$) exponents have been determined, and new relations among them have been analytically determined and empirically validated: $\rho = \gamma/\Delta$ and $\beta = \alpha\rho$. We also show evidence of universality classes for drylands. First- and second-order phase transitions coexist in the same phase diagram for distinct vegetation coverage, which allows us to unify conflicting views concerning vegetation patterns in drylands. Our findings also support the importance of terrain heterogeneity for geometrical properties of patches in MDL, mainly for small values of vegetation cover. Our results provide a way to detect early signals of desertification in drylands that is based exclusively on vegetation cover and remote sensing.

Methods

Our study examines the vegetation in drylands located in Southern Spain, within the Murcia municipality. Vegetation images were collected from Google Earth (Google 2015, 2016) from within the polygon demarcated by longitudes 1°04′00.00” W and 0°58′00.00” W and latitudes 37°58′06.00” N and 37°54′25.00” N. The images have a resolution < 40 cm. The studied region contains mountains and hills with clays and calcium-rich soil, a Mediterranean climate with semi-arid conditions, approximately 300 mm/year of precipitation (concentrated in the winter), and it has been modified by human activities for millennia. The region forms a mosaic containing farms, roads, abandoned fields, pine forests (reforestation), artificial plains and shrublands. In this study, we only considered sites formed by the typical vegetation known as “Espartales”, while all other types of formation were avoided.

The Espartales are shrublands, where the most abundant species is the alpha grass *Stipa tenacissima* L. (“Esparto”). The *Stipa* is arranged as tussocks of different sizes, alone or joined by other plant species, such as *Brachy-*

podium retusum (Pers.) P. Beauv., shrubs like *Anthylis cytisoides* L. and *Rosmarinus officinalis* L., and several chamaephytes such as *Teucrium polium* L. and *Fumana ericoides* (Cav.) Gand. The vegetation patches are mainly shrubs, almost never attaining a tree structure.

Inside the geographical polygon, we collected three sets of images, each set containing several non-overlapping and spatially independent square images (plots). The plots (images) had the pixel as the basic unit of measure. Each pixel represented the same length in meters for plots of different scales, meaning that images from different scales only differed in their total number of pixels. The ratio between the filled pixels and the total number of pixels in a plot defines its vegetation cover V. The images in distinct scales are grouped in the sets L_1 with 5×5 m^2 images, L_2 with 10×10 m^2 images and L_3 with 30×30 m^2 images. Scales of $L_i<5\times5$ m^2 could not be addressed, because smaller plots show poor patch contour resolution, while larger plots, those with $L_i>30\times30$ m^2, usually displayed some type of human-made influence. For each scale, the plots were sampled from the landscape in distinct subregions, with the aim of creating a gradient of vegetation cover, which allowed us to investigate changes in patch statistics along the V gradient. The adoption of 3 distinct scales allows the scale invariance of the aforementioned statistics to be tested.

The vegetation is distinguished from bare soil using convenient color descriptors in the ImageJ software.[29] In HSB space, we used hue and saturation contrast at their maximum values in red (Fig.2(b)). Next, we selected the brightness between 80 and 104 from each image, with most of them being around 92 (Fig.2(c)). These settings led to the best discrimination between patch edges and interpatches.[24] Next, the filtered images were transformed to binary images, where each pixel can take two values, 1 (filled by vegetation) or 0 (empty) (Fig.2(d)). Each binary image was compared with the respective original image by overlapping to confirm the quality of the patch identification. In the binary images, a cluster of filled pixels surrounded by empty pixels represents a single patch. With ImageJ analytical tools, it was possible to identify, count and measure each patch present in each plot (Fig.2(f) and (g)).

Data analysis was performed on each data set (different scales) to compare their respective results and to determine the scale dependency. In such a case, one expects that different approaches will lead to similar transition thresholds as well as critical and scaling exponents. In the vicinity of V_c, the second-order phase transition, the consistency of scaling relations between $\hat{\mu}(V)$ and $\hat{\sigma}^2(V)$ allows one to confirm the estimates of scaling exponents with empirical data. Similar conclusions are reached by relating critical and scaling exponents. In terms of percolation theory, the probability $J(V)$ estimates the probability of a random pixel (patch or interpatch) belonging to the largest patch P_{max}, while $P(V)$ is the probability of a random filled pixel belonging to P_{max}. The probabilities depicted by $J(V)$ and $P(V)$ offer an alternative way to estimate the transition thresholds,[35] confirming or rejecting the phase transition found with $D(V)$ and $\hat{\sigma}^2(V)$. It is expected that $J(V)$ will not change from $V=0$ until V_m, where it starts to increase for $V>V_m$ until $V=1$. Consequently, $J(V)$ is used to assess V_m but not V_c. The probability $P(V)$ is also interpreted as the percolation probability so that $P(V)=0$ for $V<V_m$, increasing monotonically up to $V=V_c$, where it saturates. Briefly, $J(V)$ estimates V_m, while $P(V)$ estimates V_c. Following the percolation theory approach, we introduce an estimate of vegetation connectedness in terms of a Bethe lattice. This is a first approximation that does not aim to describe the exact topology of terrain. Instead, the approach considers inferences of percolation and geometrical properties in Bethe lattices to deduce terrain influence on vegetation patterns. Accordingly, we use the coordination number z calculated from patch statistics and by theoretical predictions[30] to determine the patch connectivity, and then to infer the constraints imposed by the terrain on patch formation. Therefore, the coordination number is used to infer the influence of terrain disorder on vegetation spatial pattern. For instance, a homogeneous terrain, where patches grow in all subregions, would show high connectivity. Instead, a terrain showing constraints for plant growth would tend to show lower connectivity, because some subregions cannot

support vegetation growth.

The preliminary test with data from Utah, US, aims to explore the possibility of universality classes. Similar to MDL, rains are scarce in Utah ($\approx 300mm/year$), soils are calcium rich and the landscape is dominated by hills and valleys. However, the vegetation physiognomies found in the two regions show important contrasts. Beyond differences in species composition, patches from Utah's plots are formed by trees associated with shrubs. Consequently, patches are structurally more complex in Utah than in MDL. We concern the coordinates used in Xu *et al.*,[18] latitude $37°30'13.10"N$ and longitude $112°01'20.99"O$, to define a region of search for data acquiring. We employed the same methods used in MDL to select 36 plots of $A_i = L_i \times L_i$, with $L_i = 50m$ and to obtain patch statistics. However, resource limitations and the impossibility of field validation restricted us to employ less rigorous human supervised steps when compared with MDL. Due to the same reason, we could not explore the entire phase diagram of drylands from Utah, and all efforts are focused on the determination of the critical transition and respective critical exponents.

References

1. Rietkerk, M., Dekker, S. C., de Ruiter, P. C. & van de Koppel, J. Self-organized patchiness and catastrophic shifts in ecosystems. *Science* **305**, 1926–1929 (2004).
2. von Hardenberg, J., Kletter, A. Y., Yizhaq, H., Nathan, J. & Meron, E. Periodic versus scale-free patterns in dryland vegetation. *Proceedings of the Royal Society of London B: Biological Sciences* rspb20092208 (2010).
3. Kéfi, S. *et al.* Early warning signals of ecological transitions: methods for spatial patterns. *PloS one* **9**, e92097 (2014).
4. Tongway, D. & Hindley, N. Landscape function analysis. *Procedures for monitoring and assessing landscapes. CSIRO Sustainable Ecosystems, Canberra* (2004).
5. Bautista, S., Mayor, A. G., Bourakhouadar, J. & Bellot, J. Plant spatial pattern predicts hillslope runoff and erosion in a semiarid mediterranean landscape. *Ecosystems* **10**, 987–998 (2007).
6. Meron, E., Yizhaq, H. & Gilad, E. Localized structures in dryland vegetation: forms and functions. *Chaos: An Interdisciplinary Journal of Nonlinear Science* **17**, 037109 (2007).
7. Kéfi, S., Dakos, V., Scheffer, M., Van Nes, E. H. & Rietkerk, M. Early warning signals also precede non-catastrophic transitions. *Oikos* **122**, 641–648 (2013).
8. Abu Hammad, A. & Tumeizi, A. Land degradation: socioeconomic and environmental causes and consequences in the eastern mediterranean. *Land Degradation & Development* **23**, 216–226 (2012).
9. Low, P. Economic and social impacts of desertification, land degradation and drought. In *White Paper I, UNCCD 2nd Scientific Conference* (2013).
10. Kéfi, S., Alados, C. L., Chaves, R., Pueyo, Y. & Rietkerk, M. Is the patch size distribution of vegetation a suitable indicator of desertification processes? comment. *Ecology* **91**, 3739–3742 (2010).
11. Maestre, F. T. & Escudero, A. Is the patch size distribution of vegetation a suitable indicator of desertification processes? *Ecology* **90**, 1729–1735 (2009).
12. Kéfi, S. *et al.* Spatial vegetation patterns and imminent desertification in mediterranean arid ecosystems. *Nature* **449**, 213–217 (2007).
13. Scanlon, T. M., Caylor, K. K., Levin, S. A. & Rodriguez-Iturbe, I. Positive feedbacks promote power-law clustering of kalahari vegetation. *Nature* **449**, 209–212 (2007).

14. Moreno-de las Heras, M., Saco, P. M., Willgoose, G. R. & Tongway, D. J. Assessing landscape structure and pattern fragmentation in semiarid ecosystems using patch-size distributions. *Ecological Applications* **21**, 2793–2805 (2011).

15. Jeltsch, F. *et al.* Resilience, self-organization, complexity and pattern formation. In *Patterns of Land Degradation in Drylands*, 55–84 (Springer, 2014).

16. Pascual, M. & Guichard, F. Criticality and disturbance in spatial ecological systems. *Trends in ecology & evolution* **20**, 88–95 (2005).

17. Kéfi, S. *et al.* Robust scaling in ecosystems and the meltdown of patch size distributions before extinction. *Ecology letters* **14**, 29–35 (2011).

18. Xu, C. *et al.* Can we infer plant facilitation from remote sensing? a test across global drylands. *Ecological Applications* **25**, 1456–1462 (2015).

19. Pascual, M., Roy, M., Guichard, F. & Flierl, G. Cluster size distributions: signatures of self–organization in spatial ecologies. *Philosophical Transactions of the Royal Society of London B: Biological Sciences* **357**, 657–666 (2002).

20. D'Odorico, P., Laio, F. & Ridolfi, L. Patterns as indicators of productivity enhancement by facilitation and competition in dryland vegetation. *Journal of Geophysical Research: Biogeosciences* **111** (2006).

21. HilleRisLambers, R., Rietkerk, M., van den Bosch, F., Prins, H. H. & de Kroon, H. Vegetation pattern formation in semi-arid grazing systems. *Ecology* **82**, 50–61 (2001).

22. Vetter, S. Rangelands at equilibrium and non-equilibrium: recent developments in the debate. *Journal of Arid Environments* **62**, 321–341 (2005).

23. Xu, C., Van Nes, E. H., Holmgren, M., Kéfi, S. & Scheffer, M. Local facilitation may cause tipping points on a landscape level preceded by early-warning indicators. *The American Naturalist* **186**, E81–E90 (2015).

24. Meloni, F., Granzotti, C. R. F., Bautista, S. & Martinez, A. S. Scale dependence and patch size distribution: clarifying patch patterns in mediterranean drylands. *Ecosphere* **8** (2017).

25. Berdugo, M., Kéfi, S., Soliveres, S. & Maestre, F. T. Plant spatial patterns identify alternative ecosystem multifunctionality states in global drylands. *Nature Ecology & Evolution* **1**, 0003 (2017).

26. Stanley, H. E. Phase transitions and critical phenomena. *Clarendon, Oxford* 9 (1971).

27. von Hardenberg, J., Meron, E., Shachak, M. & Zarmi, Y. Diversity of vegetation patterns and desertification. *Physical Review Letters* **87**, 198101 (2001).

28. Binney, J. J., Dowrick, N. J., Fisher, A. J. & Newman, M. *The theory of critical phenomena: an introduction to the renormalization group* (Oxford University Press, Inc., 1992).

29. Schneider, C. A., Rasband, W. S. & Eliceiri, K. W. Nih image to imagej: 25 years of image analysis. *Nature methods* **9**, 671 (2012).

30. Solé, R. V. *Phase transitions.* Primers in complex systems (Princeton University Press, Princeton, NJ, 2011).

31. Sahimi, M. *Applications of percolation theory* (CRC Press, 1994).

32. Kadanoff, L. P. *et al.* Static phenomena near critical points: theory and experiment. *Reviews of Modern Physics* **39**, 395 (1967).

33. Meron, E., Gilad, E., von Hardenberg, J., Shachak, M. & Zarmi, Y. Vegetation patterns along a rainfall gradient. *Chaos, Solitons & Fractals* **19**, 367 – 376 (2004). DOI http://dx.doi.org/10.1016/S0960-0779(03)00049-3. Fractals in Geophysics.

34. Gilad, E., Shachak, M. & Meron, E. Dynamics and spatial organization of plant communities in water-limited systems. *Theoretical population biology* **72**, 214–230 (2007).

35. Corrado, R., Cherubini, A. M. & Pennetta, C. Early warning signals of desertification transitions in semiarid ecosystems. *Physical Review E* **90**, 062705 (2014).

36. Lefever, R., Barbier, N., Couteron, P. & Lejeune, O. Deeply gapped vegetation patterns: On crown/root allometry, criticality and desertification. *Journal of Theoretical Biology* **261**, 194 – 209 (2009). DOI http://dx.doi.org/10.1016/j.jtbi.2009.07.030.

37. Deblauwe, V., Couteron, P., Lejeune, O., Bogaert, J. & Barbier, N. Environmental modulation of self-organized periodic vegetation patterns in sudan. *Ecography* **34**, "990 – 1001" (2011).

38. Mayor, Á. G. *et al.* Feedbacks between vegetation pattern and resource loss enhance degradation potential in drylands. In *EGU General Assembly Conference Abstracts*, vol. 15 of *EGU General Assembly Conference Abstracts*, EGU2013–11852 (2013).

39. Aguiar, M. R. & Sala, O. E. Patch structure, dynamics and implications for the functioning of arid ecosystems. *Trends in Ecology & Evolution* **14**, 273–277 (1999).

40. Cardy, J. *Scaling and renormalization in statistical physics*, vol. 5 (Cambridge university press, 1996).

41. Amit, D. J. & Martin-Mayor, V. *Field theory, the renormalization group, and critical phenomena: graphs to computers* (World Scientific Publishing Co Inc, 2005).

42. Manor, A. & Shnerb, N. M. Facilitation, competition, and vegetation patchiness: from scale free distribution to patterns. *Journal of theoretical biology* **253**, 838–842 (2008).

43. Berdugo, M. Deciphering spatial patterns. can the spatial arrangement of dryland vegetation inform us about alternative states in ecosystem functioning? URL https://natureecoevocommunity.nature.com/users/25068-miguel-berdugo/posts/14328-signs-in-the-patch-can

44. Mayor, Á. G., Bautista, S. & Bellot, J. Factors and interactions controlling infiltration, runoff, and soil loss at the microscale in a patchy mediterranean semiarid landscape. *Earth Surface Processes and Landforms* **34**, 1702–1711 (2009).

45. Urgeghe, A. M. & Bautista, S. Size and connectivity of upslope runoff-source areas modulate the performance of woody plants in mediterranean drylands. *Ecohydrology* **8**, 1292–1303 (2015).

Acknowledgements

We are grateful for L.S. dos Santos' comments during the manuscript preparation. F.M. thanks S. Bautista for the hospitality during the first stages of the research. A.S.M. holds grants from CNPq 307948/2014-5, and C.R.F.G. acknowledges support from CAPES. This work was supported by the São Paulo Research Foundation (FAPESP) Grant No. 2013/06196-4 and Grant No. 2014/00631-3.

Author contributions statement

F.M. collected data and conceived the first insights about statistics and the percolation process. G.M.N. conceived the theoretical framework and the relationship between the critical exponents. F.M. and G.M.N. conducted the

numerical analysis. All authors contributed to interpreting the results and substantiating the arguments. F.M., G.M.N, and C.R.F.G. wrote the first version of the manuscript. A.S.M led the work since the early stages and edited the final version of the manuscript. All authors reviewed the manuscript.

Additional Information

The authors declare no competing financial interests.